

1 **Increasing Daytime Stability Enhances Downslope Moisture Transport in the**
2 **Subcanopy of an Even-aged Conifer Forest in Western Oregon, USA**
3

4 **S. A. Drake^{1,2}, D. E. Rupp^{2,3}, C. K. Thomas^{2,4}, H. J. Oldroyd⁵, M. Schulze⁶, and J. A. Jones²**

5 ¹Department of Physics, University of Nevada, Reno, Reno, Nevada, 89557, USA.

6 ²College of Earth, Ocean, and Atmospheric Sciences, Oregon State University, Corvallis,
7 Oregon, 97331, USA.

8 ³Oregon Climate Change Research Institute, College of Earth, Ocean, and Atmospheric
9 Sciences, Oregon State University, Corvallis, Oregon, 97331, USA.

10 ⁴Micrometeorology, University of Bayreuth, Bayreuth, Germany.

11 ⁵Department of Civil and Environmental Engineering, University of California, Davis, Davis,
12 California, 95616, USA.

13 ⁶College of Forestry, Oregon State University, Corvallis, Oregon, 97331, USA.

14 Corresponding author: Stephen Drake (stephendrake@unr.edu)

15 **Key Points:**

- 16 • Summer daytime forest canopy heating produces a within-canopy inversion and
17 downslope flow isolated from above-canopy upslope airflow
- 18 • Increased canopy inversions enhance both subcanopy wind speed and downslope water
19 vapor advection
- 20 • Regional climate change may increase moisture loss by subcanopy downslope advection
21 and greater transpiration from even-aged conifer forests

22 **Abstract**

23 Mountain breezes including katabatic and anabatic flows and temperature inversions are
24 common features of forested mountain landscapes. However, the effects of mountain breezes on
25 moisture transport in forests and implications for regional climate change are not well
26 understood. A detailed instrumental study conducted from July to September 2012 in an even-
27 aged conifer forest in the Oregon Cascade Range was investigated to determine how temperature
28 profiles within the forest canopy influenced atmospheric surface layer processes that ventilate the
29 forest. Within-canopy inversion strength has a bi-modal relationship to sub-canopy wind speed
30 and resulting moisture flux from the forest. On days with relatively modest heating of the top of
31 the canopy and weak within-canopy inversions, above canopy winds more efficiently mix
32 subcanopy air, leading to greater than average vertical moisture flux and weaker than average
33 along-slope, sub-canopy water vapor advection. On days with strong heating of the top of the
34 canopy and a strong within-canopy inversion, vertical moisture flux is suppressed, and daytime
35 downslope winds are stronger than average under the canopy. Increased downslope winds lead to
36 increased downslope transport of water vapor, carbon dioxide and other scalars under the
37 canopy. Increasing summer vapor pressure deficit in the Pacific Northwest will enhance both
38 processes: vertical moisture transport by mountain breezes when within-canopy inversions are
39 weak, and downslope water vapor transport when within-canopy inversions are strong. These
40 mountain breeze dynamics have implications for climate refugia in forested mountains, forest
41 plantations, and other forested regions with similar canopy structure and regional atmospheric
42 forcings.

43 **Plain Language Summary**

44 The summer and fall seasons in the Pacific Northwest are typically warm and dry, and solar
45 radiation and locally generated breezes affect temperature and moisture of air in the forest
46 canopy. In forest plantations, which have uniform height, canopy heating creates an inversion –
47 an increase of temperature with height under the forest canopy. On days with strong canopy
48 heating, this inversion limits moisture loss through the top of the canopy and enhances winds that
49 flow downslope below the canopy, carrying moisture out of the system. On days with less
50 canopy heating, winds mix air above and within the canopy and promote moisture loss to the air
51 above the forest canopy. Regional models of future climate simulate declining dry-season
52 relative humidity. Collectively, these findings indicate that future climate will enhance both
53 vertical and downslope moisture loss during the dry season from forest plantations, which
54 represent a large fraction of forest cover of the Pacific Northwest of the US.

55 **1 Introduction**

56 An increasing fraction of global forest area consists of plantation forests (Hansen et al.,
57 2013). Plantations typically are even-aged, with a single species and simple canopy structure
58 (Lefsky et al., 1999). Past management practices have led to millions of acres of dense, uniform
59 stands on federal forests and private land in the Pacific Northwest (PNW) where conifer forests
60 are the predominant land-cover in mountainous terrain. Several recent studies have reported that
61 even-aged conifer forests evapotranspire more water than reference, native, multi-storied forests
62 during the dry summers in the Pacific Northwest and British Columbia, Canada (Perry & Jones,
63 2017; Gronsdaahl et al., 2019; Segura et al., 2020), with potential implications for regional water
64 supply (Jones & Hammond, 2020). Yet despite the important role of forest plantations in

65 mediating land cover responses to climate change, the effects of forest plantation canopy
66 structure on atmospheric flows of heat and moisture are not well understood.

67 Forest canopy structure affects through-canopy mixing and therefore sensible heat and
68 moisture fluxes (Freundorfer et al., 2019; Thomas et al., 2013). Studies have shown that
69 maximum air temperature and vapor pressure deficit are lower under forest canopies than nearby
70 unforested areas (Karlsson, 2000; Ferrez et al., 2011). The forest water balance plays a key role
71 in buffering forest response to warming and increased vapor pressure deficit (Davis et al., 2019).
72 Regional climate processes and local terrain produce areas of relatively cool temperature in
73 forested mountains, which have been described as “microrefugia” (Dobrowski et al., 2011;
74 Lenoir et al., 2017). Many recent studies have attempted to model sub-canopy temperature (e.g.,
75 Holden et al., 2016; Lembrechts and Lenoir, 2020). Yet observational studies of heat and
76 moisture transfer in forest canopies are lacking (de Frenne et al., 2021; Thomas, 2011). A better
77 understanding of sub-canopy heat and moisture transport is relevant to topics as diverse as cold
78 air pooling, moisture transport and losses, and wildfires (Richie et al., 2007; Daly et al., 2010;
79 Frey et al., 2016; Davis et al., 2017).

80 Temperature inversions are frequent in forested mountains, even during daytime in
81 summer (Daly et al., 2010, Minder et al., 2010, Rupp et al., 2020). Landscape-scale inversions
82 and cold air pooling result from differential landscape heating (e.g., Lundquist & Pepin, 2008).
83 In addition, heating of the forest canopy influences temperature gradients and moisture exchange
84 (Brutsaert & Parlange, 1992; Leuzinger & Körner, 2007), and contributes to the formation of an
85 inversion within the canopy, especially under the uniform canopy structure of a plantation forest
86 (Hosker et al., 1974). Within-canopy inversions modulate the influence of above canopy winds
87 on the sub-canopy by limiting vertical mixing into the sub-canopy (Launiainen et al., 2007;
88 Thomas and Foken, 2007). Within-canopy inversions tend to weaken during the night
89 (Whiteman, 1982; Juang et al., 2006) and re-establish and strengthen during the day (Raynor,
90 1971; Staebler et al., 2005; Froelich and Schmid, 2006; Tóta et al., 2012). Although models have
91 explored how forest canopy structure influences air flows in mountain valleys (Kiefer & Zhong,
92 2013, 2015), few studies have examined the interaction between within canopy temperature
93 inversions and airflow within forest canopies in mountain landscapes.

94 The objective of this study is to determine how summertime heating of the canopy of a
95 dense plantation forest influences movement of heat and moisture into, out of, and within the
96 forest canopy in a steep mountain watershed, which is typical of much of the Pacific Northwest
97 of the US. The study quantified sub-canopy atmospheric processes in a 45-yr-old plantation
98 forest characterized by a uniform single-layer canopy during the summer dry season when plants
99 are drought stressed and therefore more sensitive to subtle environmental changes (Hughes,
100 2000). Subcanopy flow regimes are then examined in the context of regional climate change
101 predictions over PNW forests to investigate the feedback between canopy heating and subcanopy
102 moisture transport.

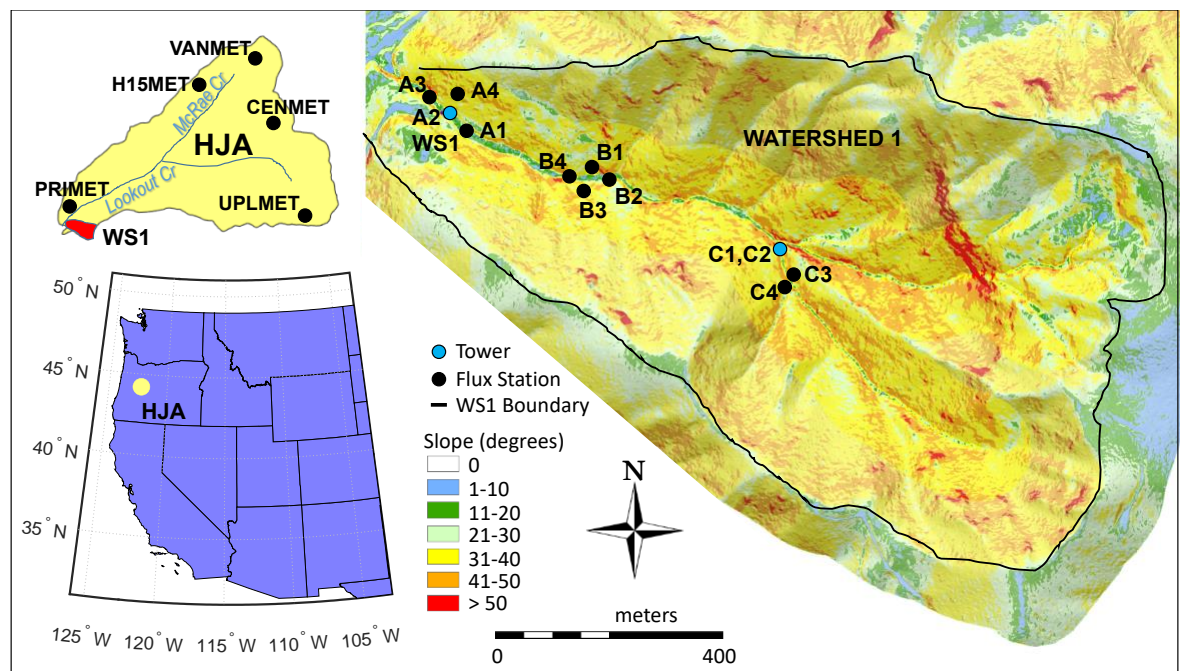
103 **2 Materials and Methods**

104 **2.1 Study site**

105 The study was conducted from July through September of 2012 in a sub-basin of Lookout
106 Creek (64 km²), in the HJ Andrews Experimental Forest (HJ Andrews) and Long-Term
107 Ecological Research (LTER) site in the central western Cascades of Oregon, USA (122.25° W,

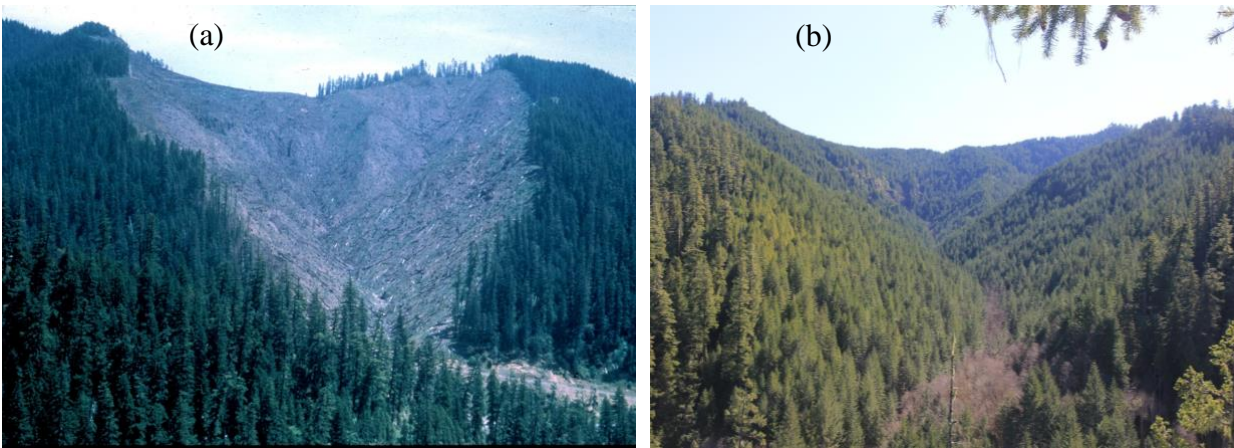
108 44.21° N). Slope gradients range from 30 to more than 60% in the HJ Andrews, and steep
 109 tributary valleys, such as the study site, drain to a central valley. Mean annual temperature is 9.7
 110 °C and mean annual precipitation is 2350 mm. Less than 5% of precipitation occurs during the
 111 dry season (July 1 – September 30) (Harr, 1983). The study site was Watershed 1 (WS1, Figure
 112 1), a relatively small (96 ha), steep (average slope ~60%) northwest facing valley near the outlet
 113 of Lookout Creek Basin. Elevation ranges from 460 to 990 m in WS1, and from 430 to >1600 m
 114 in Lookout Creek. The original vegetation of WS1, old growth Douglas-fir (*Pseudotsuga*
 115 *menziesii*) (150 to 500-yr), was clearcut and cable yarded between 1962 and 1966, and the
 116 remaining slash was subsequently broadcast burned in 1966 (Fredricksen, 1970; Perry & Jones,
 117 2017) (Figure 2). Douglas-fir was planted and aerielly seeded during the late 1960s. As of 2012,
 118 the planted forest consisted of a dense stand of ~45-yr-old Douglas-fir with deciduous red alder
 119 (*Alnus rubra*) along the stream channel (Figure 2). The average height of the canopy was 29 m,
 120 and the canopy extended down to 8 m above the ground, with understory vegetation from 1 to 4
 121 m high. Many studies in WS1 have examined post-disturbance succession, ecohydrology, and
 122 carbon budgets, and other topics (e.g.: Halpern et al., 1990; Hicks et al., 1991; Moore et al.,
 123 2004; Pypker et al., 2007; Hood et al., 2006; Argerich et al., 2016). Basal area, growth rates, and
 124 density in the forest plantation in WS1 are within reported ranges for managed and unmanaged
 125 forest plantations on steep watersheds in western Oregon (Perry & Jones, 2017).

126



127 Figure 1. Overview maps show the location of the HJ Andrews Experimental Forest in Oregon,
 128 the locations of benchmark stations and the WS1 tower within the HJ Andrews domain and flux

129 station locations within Watershed 1. (source: Theresa Valentine, Corvallis Forest Science
 130 Laboratory). The Watershed 1 stream drains into Lookout Creek 150 m below station A3.

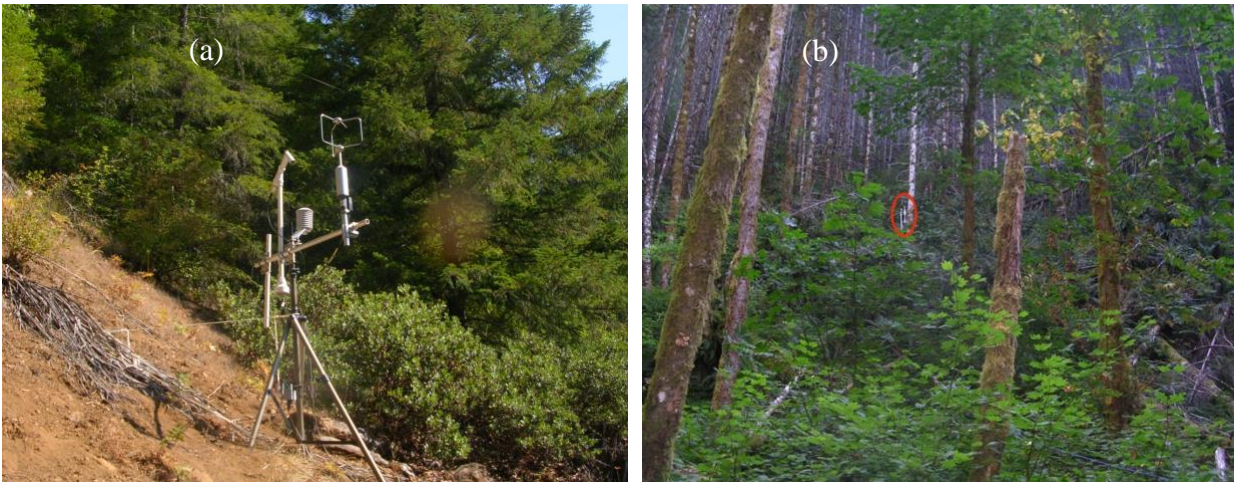


131 Figure 2. Watershed 1 viewed from the north after clear-cut in the late 1960s (panel a, Photo:
 132 Dick Fredricksen) and in 2019 (panel b, Photo: Mark Schulze).

133 2.2 Data collection

134 Air flow, heat, and moisture were measured within three sub-domains along the valley
 135 axis (Figure 1). Enclosure-mounted data loggers (Model CR3000, Campbell Scientific Inc.
 136 Logan, UT, USA) were deployed at three base sites ranging from 470 m to 580 m elevation
 137 along a ~1-km transect up the WS1 valley floor from Lookout Creek. At each base site,
 138 designated as “A”, “B”, and “C,” data were collected from four stations, labeled e.g., A1, A2, A3
 139 and A4, etc. Stations were positioned with the primary goal of measuring sub-canopy wind,
 140 temperature, and moisture along the valley axis (stations A1, A2, A3, B2, B4, C1, C2, C4) and
 141 with secondary goals of resolving winds in open locations (station A4) and drainage flow
 142 contributions from side slopes (B1, B3) and tributary channels (C3, Figure 1). Sensors were
 143 mounted on tripods at 2 m nominal height above ground level (agl) and aligned with local
 144 gravity. Sensors at sites A2, C1, and C2, were positioned higher above ground to further resolve
 145 bole-space characteristics. Here, “bole-space” is taken as the air volume between the lower
 146 fringe of the canopy and the ground. Sensors at A2 were mounted at the 16-m level of a 37-m
 147 tower designated as WS1 Tower (Figure 1). Sensors at C1 and C2 were mounted at 7.4 m and
 148 12.9 m (boom-extended) on a 12.2-m tower. All A, B and C sensors were placed within or below
 149 the canopy, except station A4, which was located in a SW-facing canopy opening on a slope 120
 150 m uphill from the WS1 tower (Figure 3a).

151



152 Figure 3. Photographs of example stations. (a) Station A4 was located in a SW-facing canopy
 153 opening on a slope 120 m uphill from the WS1 tower. (b) Station B3 was located on a forested
 154 slope and identified by a red ellipse. (Photo: Stephen Drake).

155

156 Wind speed and direction were sampled at 20 Hz using ultrasonic anemometers (Model
 157 Young VRE81000, RM Young, Traverse City, MI, USA), hereafter referred to as “sonics”. One-
 158 minute averaged temperature and humidity were measured using aspirated thermohygrometers
 159 (Model Vaisala HMP 155, Vaisala, Finland) paired with each sonic. Thermohygrometers were
 160 mounted in actively aspirated radiation shields (Thomas & Smoot, 2013) with inflow at centroid
 161 height of the sonic volume.

162 Additional sensors were mounted on the 37-m WS1 tower in order to determine within-
 163 canopy stability and to measure above canopy winds near the watershed outlet. The WS1 tower
 164 extended 4 m above the top of the canopy (33 m). Temperature was measured using aspirated
 165 thermistors (Model 107, Campbell Sci., Logan, UT, USA) mounted at 1, 7, 12, 18, 23, 29 and 37
 166 m and recorded at 1-minute averages by a datalogger (Model CR23x, Campbell Scientific,
 167 Logan, UT, USA). Tower-mounted instrumentation used in this investigation included open-path
 168 CO₂/H₂O analyzers (Model Licor LI-7500, Licor, Lincoln, NE, USA) at 4 and 37 m, an
 169 additional sonic anemometer at 4 m (Model CSAT3, Campbell Scientific, Logan, UT, USA), and
 170 a 3-axis sonic anemometer at 37 m (Model Gill R2, Gill Instruments, Lymington, UK) sampled at
 171 20 Hz and recorded by a datalogger (Model CR3000, Campbell Scientific Ltd. Logan, UT,
 172 USA).

173 Wind speed and direction, air temperature and moisture data obtained in the WS1
 174 watershed were averaged to 1-minute intervals.

175 2.3 Basin-scale and regional reanalysis data

176 Basin-scale (Lookout Creek) data of wind speed and direction for the study period were
 177 obtained from five HJ Andrews benchmark stations: PRIMET (436m), H15MET (909m),
 178 CENMET (1028 m), VANMET (1268 m) and UPLMET (1298 m) (Figure 1). Wind speed and
 179 direction are measured at 10 m (except for H15MET which was at 5 m) using propeller

180 anemometers (Model, 05103 Wind Monitor, RM Young, Traverse City, MI, USA). Data were
181 averaged to 15-minute intervals. The propeller on this anemometer has a 1 m s^{-1} minimum
182 threshold (Campbell Scientific, 2015). Sub- 1 m s^{-1} averages were kept in subsequent analyses to
183 resolve the diurnal cycle of wind speed with the potential that sub- 1 m s^{-1} measurements that
184 constitute the 15-minute averages may have systematically skewed 15-min wind averages
185 downward during periods with weak winds. The impact of this potential systematic error was
186 minimized by comparing relative changes in wind speed rather than absolute wind speed.
187 Benchmark stations are located in canopy gaps, and the sensor heights are below the surrounding
188 forest canopy, which decreased measured wind speed.

189 Regional-scale wind data for the study period were obtained from the land component
190 European Centre for Medium-Range Weather Forecasts (ECMWF) Re-Analysis 5 (Muñoz-
191 Sabater et al., 2021; Hersbach et al., 2020). This product combines observations and model
192 physics to reproduce hourly atmospheric state variables and derivatives with land surface
193 variables interpolated to grid points with $0.1^\circ \times 0.1^\circ$ resolution.

194 Spatially distributed and synchronous measurements of temperature, wind speed,
195 barometric pressure, and humidity were available for 50 of the 55 days between July 25 and Sept
196 17 for which. Data gaps occurred for three days with the 1 m temperature sensor and for two
197 days with the 4 m sonic anemometer on the WS1 tower. Hereafter, these 50 days are referred to
198 as the 50-day IOP (Intensive Observation Period).

199 2.4. Data analysis

200 To identify the persistence and timing of wind patterns, diel airflow measurements at the
201 WS1 tower were composited (averaged) to highlight features that are commonly observed during
202 the same time daily. Before compositing potential temperature profiles, observed dry-bulb air
203 temperature was converted to potential temperature by correcting for the dry-adiabatic lapse rate
204 of 9.8 K km^{-1} , accounting for temperature differences due to elevation. Individual daily plots
205 were compared with composites to verify that a single, large amplitude anomalous feature on a
206 given day did not unduly bias time composites. Daily composite data were divided into four
207 distinct time periods based on wind speed and direction following Whiteman (1990) and Pypker
208 et al. (2007). The four time periods are: daytime flow (DF), evening transition (ET), nighttime
209 conditions (NC) and morning transition (MT). During clear-sky conditions, the DF time period is
210 distinguished by thermally-driven upslope flow above the canopy. The ET time period begins
211 when above-canopy wind direction reverses and air flows downslope. The NC time period
212 begins as turbulence weakens, and NC transitions to the MT as insolation initiates upslope flow
213 above the canopy the following morning.

214 The strength and effects of the within-canopy inversions created by heating of the forest
215 canopy were examined by calculating static stability, wind speed, and latent heat flux during
216 daytime flow (DF) at the WS1 tower for the 50-day IOP. Maximum sub-canopy static stability
217 (Stull, 2012) was computed during the time period of peak canopy heating (13:30 to 14:30, local
218 time). Static stability was computed as the average potential temperature difference between the
219 1 and 23 m heights on the WS1 tower divided by the difference in height (K m^{-1}). Static stability
220 is used as a measure of sub-canopy stability rather than the stability parameter used in Wang et
221 al. (2015) because the Obukhov length is not a valid stability parameter within the roughness
222 sublayer (Vickers & Thomas, 2014), or for katabatic flow (Oldroyd et al., 2016). Bole-space
223 wind speed and direction were calculated at 4 m height on the WS1 tower for the same 13:30 to

224 14:30 time frame as static stability. Wind direction was classified into two categories: variable
 225 (all directions) and down-valley, defined as wind direction $\pm 25^\circ$ within the most prominent
 226 down-valley direction. During periods of variable winds, even if the wind has a down-valley
 227 component, intermittent turbulence and coherent structures in above canopy winds may have
 228 significantly influenced the sub-canopy wind direction during discrete events. These one-hour
 229 averages of static stability, wind speed and wind direction variability were used to characterize
 230 wind regimes as a function of subcanopy static stability.

231 Turbulence kinetic energy (TKE) is the kinetic energy, usually expressed per unit mass,
 232 associated with eddies in a turbulent flow. TKE in the sub-canopy drives the vertical exchange of
 233 moisture across the boundary from the forest canopy to the air above. Thirty-minute averaged
 234 turbulence kinetic energy (TKE) was calculated for each station as (Stull, 2012):

$$235 \quad \frac{TKE}{m} = 0.5 \left(\overline{u'^2} + \overline{v'^2} + \overline{w'^2} \right) , \quad Eq (1)$$

236 where m is mass, u' , v' , and w' are instantaneous deviations from 30-minute mean wind
 237 components and the overbar represents a 30-minute average. TKE was calculated for subcanopy
 238 stations at the 2-m nominal height of the sonic anemometers.

239 Turbulence intensity (TI) is defined as the standard deviation of wind speed, σ_M , divided
 240 by the mean wind speed, \bar{M} , (Stull, 2012):

$$241 \quad TI = \frac{\sigma_M}{\bar{M}} . \quad Eq (2)$$

242 and provides a normalized measure of turbulence.

243 To assess the relationship of within-canopy dynamics in Watershed 1 to the basin and the
 244 region, data on wind speed from benchmark stations PRIMET (430m elevation), H15MET
 245 (909m), CENMET (1020m), VANMET (1275m), and UPLMET (1295m) throughout HJ
 246 Andrews (Figure 1) were averaged for each day of the study period.

247 To assess the effect of within-canopy inversions and winds on moisture fluxes within and
 248 through the forest canopy, the difference in water vapor concentration in the sub-canopy
 249 compared with the air above the canopy was determined as water vapor concentration (mol m^{-3})
 250 at 4 m minus the water vapor concentration at 37 m, integrated over the daytime flow period, for
 251 each day of the study period, and this was related to the maximum static stability on each day.

252 To test the hypothetical effect of climate warming on sub-canopy winds and moisture
 253 transport, we calculated wind speed and virtual temperature differences between stations B4 and
 254 C4 along the main channel for days with relatively high in-canopy stability and determined the
 255 relationship between these air temperature and wind speed differences between these two sites.
 256 We then used this relationship to determine the effect of a 0.1 K m^{-1} increase in static stability on
 257 downslope water vapor transport by subcanopy winds. As in prior studies from this site (i.e.,
 258 Pypker et al., 2007), downslope moisture transport is computed at the airshed exit although
 259 localized moisture fluxes are also present within the watershed boundary where moisture
 260 gradients are present.

261 3 Results

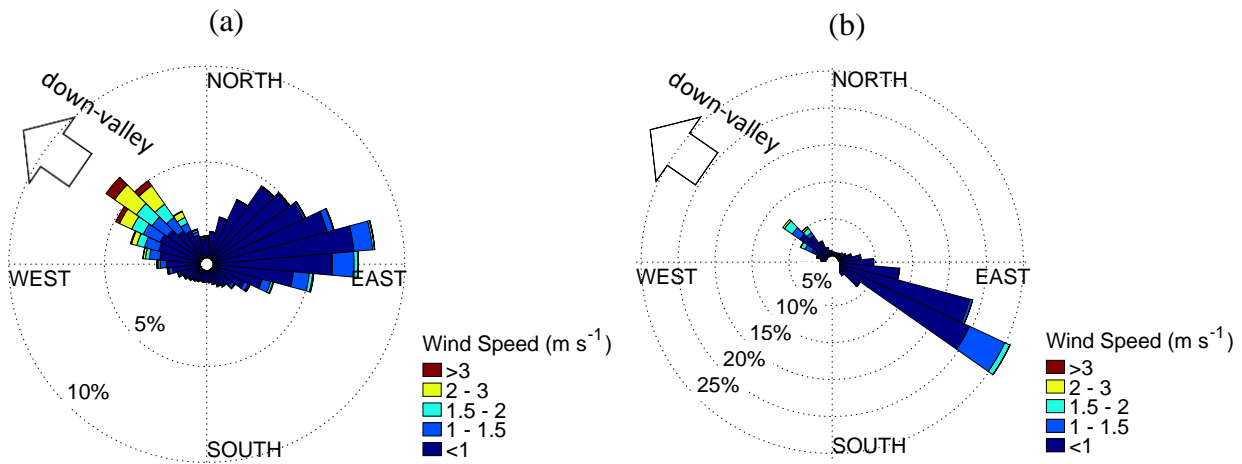
262 Above and sub-canopy wind speed and direction are composited for the experimental
263 period in Sections 3.1 and 3.2 to summarize the local wind patterns. Winds are then categorized
264 into four daily time periods (Section 3.3). We examine how inversion strength (static stability) is
265 related to wind speed and how turbulence and latent heat flux varies over the day, above and
266 below the canopy, for low-stability and high-stability conditions (Section 3.4). We show that on
267 days with high static stability, the downslope subcanopy wind speed increases with stability, and
268 low-stability days are associated with higher turbulence intensity but lower temperature below
269 the canopy (Section 3.5). The coherence of sub-canopy wind and above-canopy winds within the
270 larger Lookout Creek basin are investigated in Section 3.6. In Section 3.7 results indicate that
271 stronger within-canopy inversions are associated with greater sub-canopy humidity, relative to
272 the air above the canopy, and these stronger within-canopy inversions (on high-stability days)
273 constrain within-canopy mixing and vertical moisture flux out of the canopy relative to low-
274 stability days. Finally, we use the relationship of wind speed and virtual temperature differences
275 between stations B4 and C4 along the main channel for high-stability days to test the
276 hypothetical effect of warming on sub-canopy winds and moisture transport (Section 3.8).

277 Summer and fall seasons in the PNW are typically dry, dominated by a persistent high
278 pressure synoptic pattern. However, June 2012 antecedent conditions in the HJ Andrews region
279 were very moist with a Palmer Z index between 2.5 and 3.5 (NOAA NCDC Annual Drought
280 Report, 2012, see also supplement section S1). During the study period (July 19, 2012 to
281 September 17, 2012), Oregon ranked as the 2nd driest state and much of the continental US
282 experienced drought conditions throughout this time period. Consequently, the progressive
283 decrease in latent heat flux between the beginning of July and end of September was
284 representative for a drought index transition from very moist to severe drought conditions. The
285 prolonged dry period during the study period provided favorable conditions for isolating the
286 effects of within-canopy stability on sub-canopy moisture transport.

287 3.1 Above vs. below-canopy winds

288 Based on 1-minute averaged data acquired from July 25 to Sept 17, 2012, wind above the
289 canopy at WS1 tower had two prominent directions: from the NW and from the ENE (Figure
290 4a). The strongest winds were from the NW due predominantly to up-valley daytime flow and
291 topographic steering rather than synoptic forcing at this locale (see also Figure S2 with overview
292 of synoptic forcing in the supplement). Above the canopy, weaker down-valley (Lookout Basin)
293 and down-slope winds from the eastern portion of the Watershed 1 basin were common during
294 nighttime throughout the study. Wind above the canopy was more variable than below the
295 canopy, in part due to 3-dimensional vorticity of turbulent eddies at the time scale of 1-minute
296 averages. In contrast, wind direction below the canopy at 4-m height was bimodal, aligning with
297 the watershed axis (Figure 4b). Sub-canopy wind direction along the valley axis was primarily
298 down-valley throughout the day (Figure 4b). The consistently lower speed and more directional
299 winds at 4 m compared to 37 m indicate that the canopy acts as a permeable mechanical and
300 thermodynamic barrier that dampens through-canopy turbulent fluxes.

301



302

303

304 Figure 4. Windroses on WS1 tower color-coded by wind speed at 37 m AGL (above canopy,
 305 panel a) and at 4 m AGL (below canopy, panel b).

306

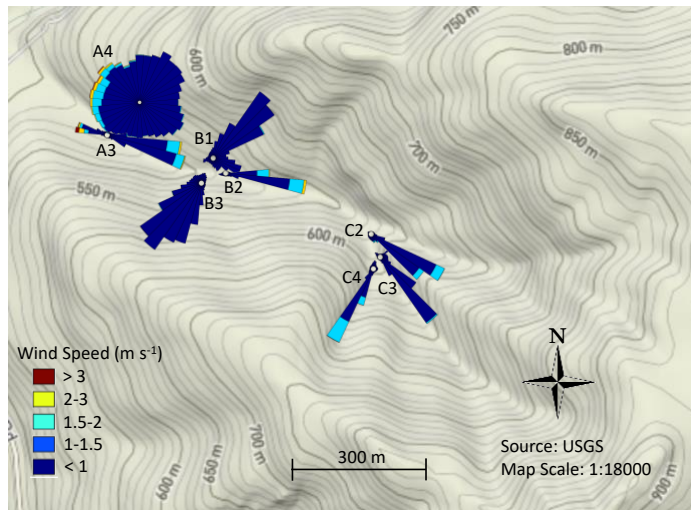
307 3.2. Wind patterns as a function of canopy cover and position within the watershed

308 Below the canopy (2 m), downslope winds occurred throughout the watershed during
 309 both daytime and nighttime. The relative frequency of downslope flow varied by position in the
 310 watershed and by canopy cover (Figure 5). Below-canopy winds were primarily downvalley
 311 throughout the day at sites located along the axes of tributaries in the upper valley (C2, C3, C4)
 312 and at sites aligned with the channel axis in the mid-valley (B2 and B4). In contrast, below-
 313 canopy wind direction was primarily downslope at sites positioned slightly higher above the
 314 valley axis (B1 and B3); these sites were dominated by downslope rather than down-valley flow
 315 because they were positioned generally above the depth of down-valley cold air drainage flows.
 316 In addition, wind direction was quite variable at a location having a canopy opening (site A4,
 317 Figures 3a and 5); this site was exposed to above-canopy winds, multi-scale forcing, edge effects
 318 and turbulence, which disrupt the nocturnal/downslope, daytime/upslope wind regime.

319

320

321



322 Figure 5. Windroses of 1-minute averaged winds at 2 m nominal height for subcanopy stations
 323 A3, A4, B1, B2, B3, C2, C3 and C4 in Watershed 1. Stations A1 and B4 have very similar
 324 windrose shapes as station A3 in Figure 5 but are not rendered to avoid overlapping. Windrose
 325 bin sizes are rescaled to avoid overlap and highlight features described in the text. (Map source
 326 USGS)

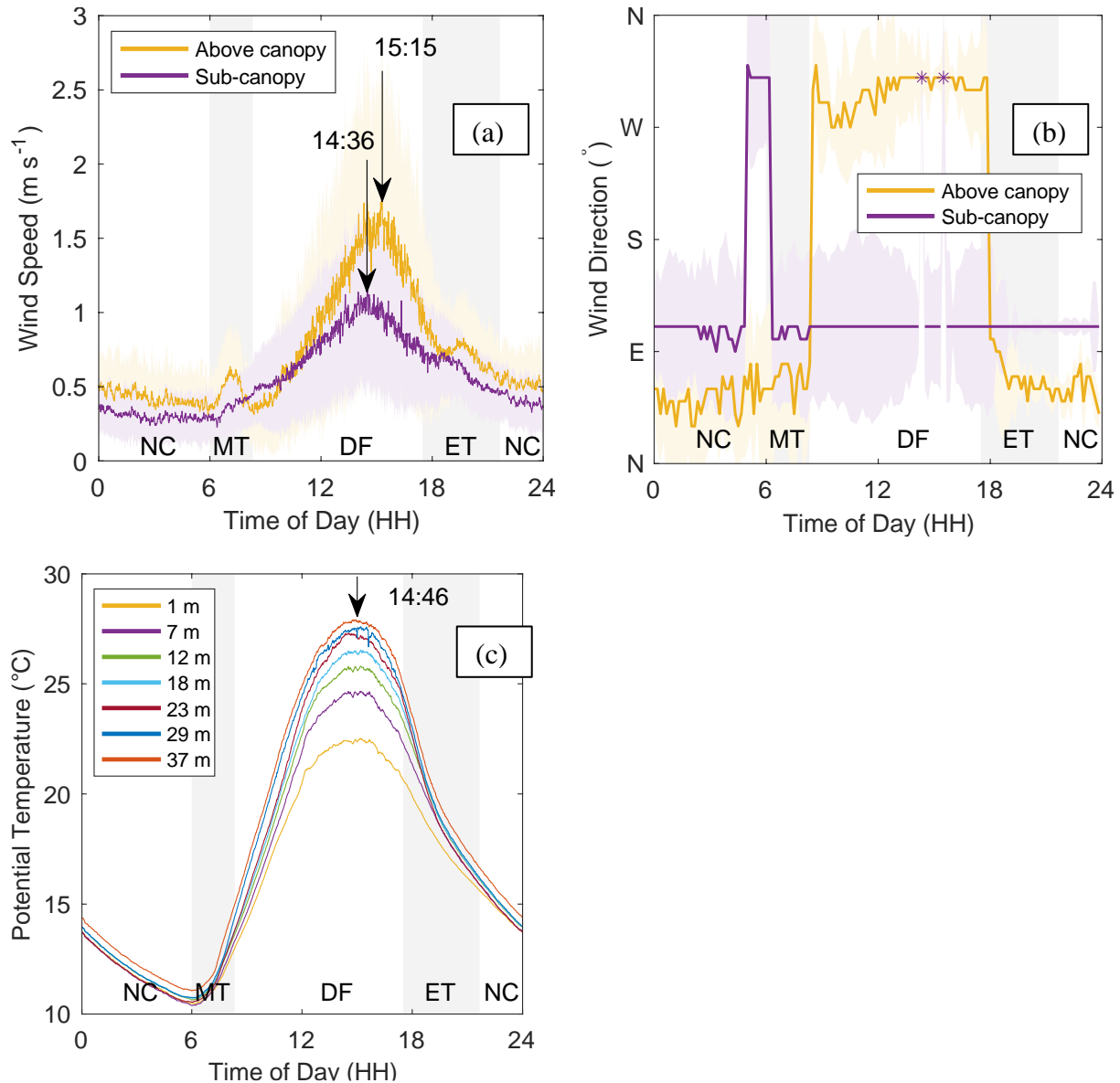
327

328 3.3 Four time periods of wind

329 Average wind speed and direction at the WS1 tower clearly display four time periods of:
 330 morning transition, daytime flow, evening transition, and nighttime conditions (Figure 6a). After
 331 the morning transition (MT), wind speed above and below the canopy increases during the
 332 daytime flow period and gradually diminishes throughout the nighttime conditions period
 333 (Figure 6a). During the morning transition, solar heating in Lookout Creek Basin erodes the cold
 334 air pool and sub-canopy gravity-driven flow increases following a brief, weak wind direction
 335 reversal (Figure 6b). This sub-canopy MT wind reversal is likely caused by a pressure gradient
 336 adjustment during the transition from the nighttime conditions to daytime flow (NC to DF)
 337 period and is characteristic of transition periods in mountainous regions (Nadeau et al. 2012;
 338 Nadeau et al. 2018). Above the canopy, downslope winds exhibit a local maximum in magnitude
 339 during MT (Figure 6a), as solar heating in Lookout Creek Basin initiates a mountain breeze that
 340 precedes solar heating in the Watershed 1 basin (see also Section 3.6).

341 The maximum inversion (5.6 °C difference in temperature at 37 m vs. 1 m) occurred at
 342 14:46, consistent with canopy heating by solar insolation (Figure 6c). During the daytime flow
 343 (DT), the sub-canopy wind speed peaks at 14:36, about 10 minutes before the time of maximum
 344 temperature inversion within the canopy, whereas the above-canopy wind speed peaks at 15:15,
 345 about 29 minutes after the time of maximum inversion (Figures 6a, 6c). During the evening
 346 transition (ET), wind directions roughly align above and below the canopy as nocturnal drainage
 347 flow reestablishes above the canopy. Gravity flow decreases throughout the night, as nocturnal
 348 drainage flow fills the valley with cold air, until the morning transition and the diurnal cycle
 349 repeats.

350



351 Figure 6. Composite wind speed (a), wind direction (b) and potential temperature for heights
 352 ranging from 1 to 37 m (c) at the WS 1 tower for the period July 19, 2012 to Sept. 17, 2012, and
 353 four flow regimes (vertical white and grey bars): daytime flow (DF), evening transition (ET),
 354 nighttime conditions (NC) and morning transition (MT). Flow regimes are defined as in
 355 Whiteman (1990) and Pypker et al. (2007). Wind speed is shown above the canopy at 37 m
 356 (gold) and below the canopy 4 m (purple) (panel a) with time of peak winds delineated by
 357 arrows. Composite wind directions are defined by the mode of wind direction at each minute in
 358 10-degree bins (panel b). Shading indicates one standard deviation. Purple asterisks in panel (b)
 359 indicate two short time periods when the subcanopy wind direction mode at the WS1 tower was
 360 preferentially upvalley.

361 The sub-canopy diurnal wind direction response in the WS1 basin (Figures 5 and 6) is
 362 different from the archetypal mountain breeze regime. An archetypal, thermally-driven mountain

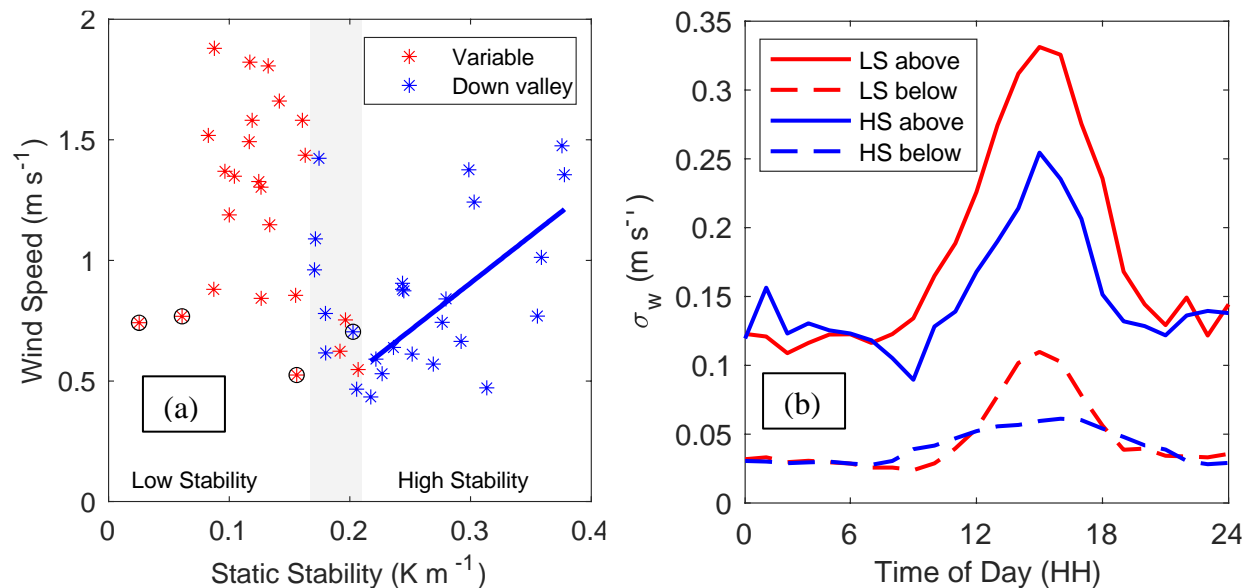
363 breeze presents upslope flow during the DF period that increases with increased heating
 364 (Schmidli, 2013). In contrast, along the valley axis the dominant subcanopy wind direction was
 365 down-valley (Figure 5), and the highest sub-canopy wind speeds were downvalley at
 366 representative stations along the valley axis (Figure 6a, 6b). These differences appear to be due
 367 to the presence of an even-aged dense forest canopy, which creates an inversion that modulates
 368 below-canopy air flows.

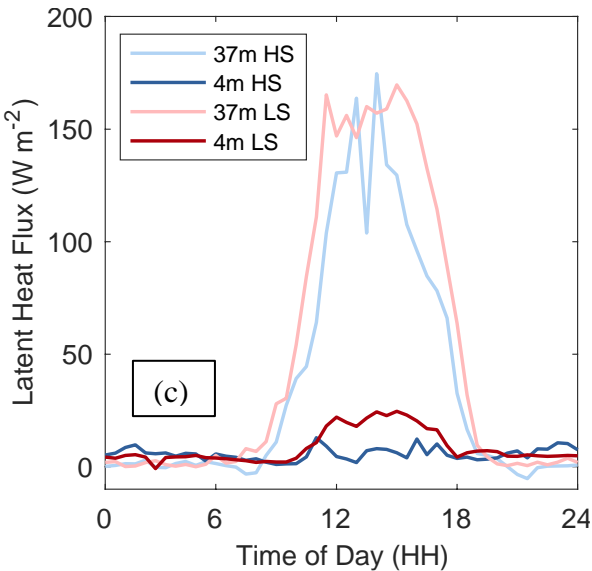
369 3.4 Daytime flow mode

370 Over the 50-day IOP the relationship of 4 m sub-canopy wind speed to static stability
 371 differs below and above a stability transition zone (grey bar in Figure 7a). For days with static
 372 stability values below 0.17 K m^{-1} , wind speed is not correlated with stability (red data points,
 373 $R^2=0.04$). For days with static stability values above 0.21 K m^{-1} , down-valley wind speed
 374 increases with increasing static stability (blue data points, $R^2=0.42$). Other factors, such as the
 375 coherence of diel pressure gradient evolution and shortwave solar insolation also influence wind
 376 speed (Figures S3 and S4 in the supplement).

377 The standard deviation of vertical wind speed, σ_w , was greater during low stability
 378 compared with high stability days, both above and below the canopy (Figure 7b), indicating
 379 greater potential for vertical mixing on low-stability days. The standard deviation of vertical
 380 wind speed was many times higher above than below the top of the canopy (Figure 7b). Below
 381 the canopy, the low stability maximum σ_w (~ 0.1) was twice the high stability value (~ 0.05),
 382 while above the canopy, the low stability maximum σ_w (0.33) was 33% greater than the high
 383 stability value (0.25). These findings, combined with the relationship of wind speed to stability
 384 (Figure 7a), indicate that within-canopy mixing was suppressed on high-stability days relative to
 385 low-stability days. The likely physical mechanism for this σ_w reduction is the enhanced
 386 temperature inversion on high stability days, because the buoyancy restoration force has larger
 387 magnitudes in stably stratified fluids (Vickers & Thomas, 2013).

388

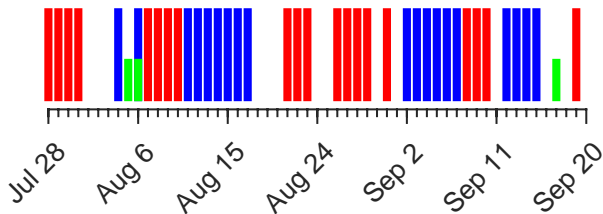




389 Figure 7. Relationship of composite 4 m wind speed to static stability (a); composite σ_w over the
 390 day (b); and composite latent heat flux over the day (c). Panel (a) shows WS1 tower 4-m mean
 391 wind speed vs. canopy static stability over the 1 to 23-m layer during the time period 13:30 to
 392 14:30 for each of the 50-day IOP. Wind speed is coded by dominant daily wind direction
 393 (variable = red, or downvalley= blue). Overcast days are circled. (b) Composite standard
 394 deviation of the vertical wind speed component by time of day computed at 37 m (above canopy)
 395 and 4 m (below canopy) heights for low static stability (LS) and high static stability (HS)
 396 days indicated in panel (a). (c) Composite latent heat flux at 4-m and 37 m heights for LS and HS
 397 days.

398 These effects on vertical mixing produce much higher latent heat fluxes just above the
 399 canopy compared to within the canopy, and 26% greater vertical moisture loss via mixing during
 400 low-stability compared to high-stability days just above the canopy (37 m) (Figure 7c). But for
 401 brief spikes at 13:00 to 15:00 on high-stability days, latent heat fluxes at 37 m were higher
 402 throughout the DF period during low-stability days compared with high-stability days, indicating
 403 more continuous through-canopy mixing on low-stability compared with high-stability days.

404 The finding of distinctly different DF flow regimes permit classifying days in the 50-day
 405 IOP according to their daytime flow values of static stability and associated moisture flux
 406 characteristics (Figure 8). Twenty-one of the 50 days were low-stability, 19 were characterized
 407 as high-stability and 10 days were transitional. Low- and high-stability periods tend to persist for
 408 several consecutive days.



409 Figure 8. Days in the 50-day IOP classified as low-stability (red) or high-stability (blue), based
410 on analysis in Figure 7a. Days with precipitation are shown in green.

411 Atmospheric conditions that differentiate low-stability from high-stability days are examined in
412 the supplement. A distinguishing characteristic of HS days is synchronicity of the pressure
413 tendency that is lacking on LS days. As will be shown in Section 3.6, the basin-wide, daytime
414 change in wind speed is smaller on HS days relative to LS days.

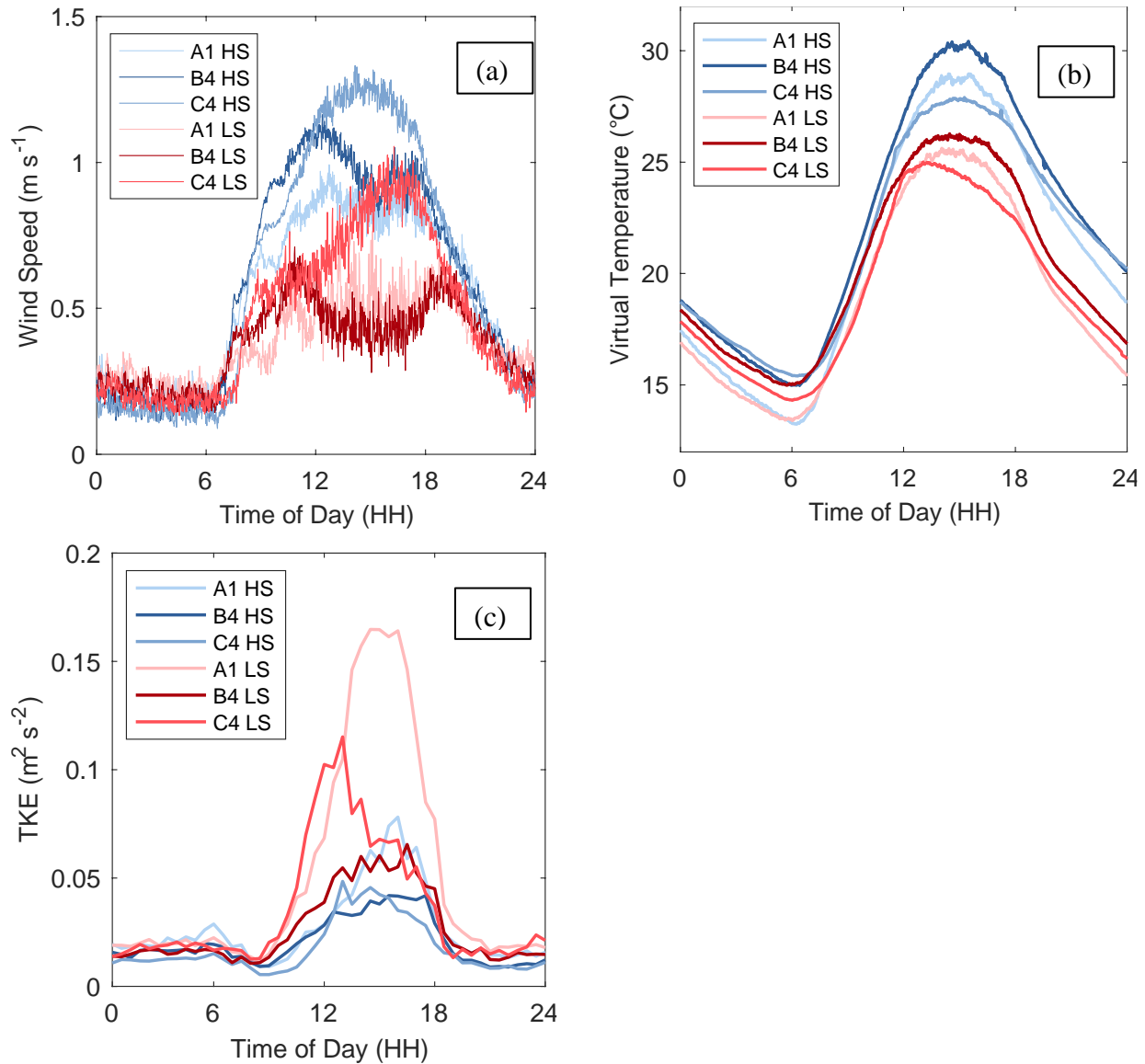
415 3.5 Along-valley wind characteristics

416 Subcanopy wind speed during daylight hours in the July 25 to Sept 17 study period was
417 consistently higher on high-stability days than on low-stability days at the three stations along
418 the Watershed 1 valley axis (A1, B4, C4) (Figure 9a). Wind speed also was more variable during
419 LS days (shades of red in Figure 9a) than HS days. Composite virtual temperature (T_v) was also
420 greater on HS compared with LS days at stations A1, B4 and C4 (Figure 9b). Lower sub-canopy
421 T_v during LS days compared with HS days may be the result of a weaker inversion and greater
422 prevalence of large, coherent eddies on LS days that inject relatively dry above-canopy air into
423 the sub-canopy. Several overcast days (Figure 7a, Figure S4) also contributed to lower ensemble
424 sub-canopy T_v during LS days.

425 During the afternoon on HS days, air at station C4 (an upstream tributary) was denser
426 (had a lower T_v) than at B4 or A1 (in the main channel) (Figure 9b). Denser air increased
427 katabatic acceleration at C4 relative to B4 or A1, producing the higher wind speed observed at
428 C4 compared with A1 or B4 (Figure 9a). Even for LS days, a katabatic signature was evident at
429 station C4 where increased afternoon cooling relative to stations A1 and B4 was associated with
430 an increase in afternoon wind speed (Figures 9a, 9b). On the other hand, on HS days T_v and wind
431 speed at midday were higher at B4 (axis of main channel, midway down the valley) than A1
432 (axis of main channel, near mouth of the watershed), counter to the density effect on katabatic
433 acceleration. This discrepancy could be attributed to mass continuity and the widening of the
434 valley floor at A1, which increases sub-canopy volume thereby slowing sub-canopy winds.
435 Differences in subcanopy roughness and canopy elements between stations also may be a
436 contributing factor in the observed differences in subcanopy wind speed (Thomas, 2011), despite
437 efforts to locate stations to minimize along-slope flow disruption by vegetation.

438 Turbulence kinetic energy was higher during daylight hours, higher on low-stability
439 compared to high-stability days, and higher at stations A1 (valley mouth) and C4 (upper valley)
440 than B4 (midway down the valley) (Figure 9c). Station B4 had relatively low TKE on both LS
441 and HS days whereas station A1 exhibited the highest TKE for all days. As before, high
442 variability in wind speed and enhanced TKE generation can be attributed to proximity of station
443 A1 to the WS1 airshed outlet to Lookout Creek. Relatively low subcanopy wind speeds (Figure
444 9a) coincided with relatively high TKE on LS days at A1, and the highest average composite
445 wind speed coincided with the lowest average composited TKE at 1500-1800h on HS days at
446 station C4 (Figure 9c). While increased wind speeds, which at these subcanopy sites occur with
447 the HS condition, are typically related to high shear generation, higher stability likely suppresses
448 vertical TKE transport across the canopy. This result is consistent with Figure 7b, which showed
449 that on LS days above canopy winds ventilate the subcanopy and large eddies introduce TKE
450 into the subcanopy environment. Below the canopy, vertical mixing is enhanced along the valley
451 axis on LS days and suppressed on HS days.

452
453
454



455 Figure 9. Comparing sub-canopy wind speed during HS and LS days at selected stations in WS1
456 (panel a). In panel (b), sub-canopy 1-minute averaged virtual temperatures and in panel (c) 30-
457 minute averaged TKE are compared at the same stations as in panels (a) and (b) for HS and LS
458 days. All measurements were obtained at 2-m nominal height agl.

459 3.6 Basin-scale wind patterns

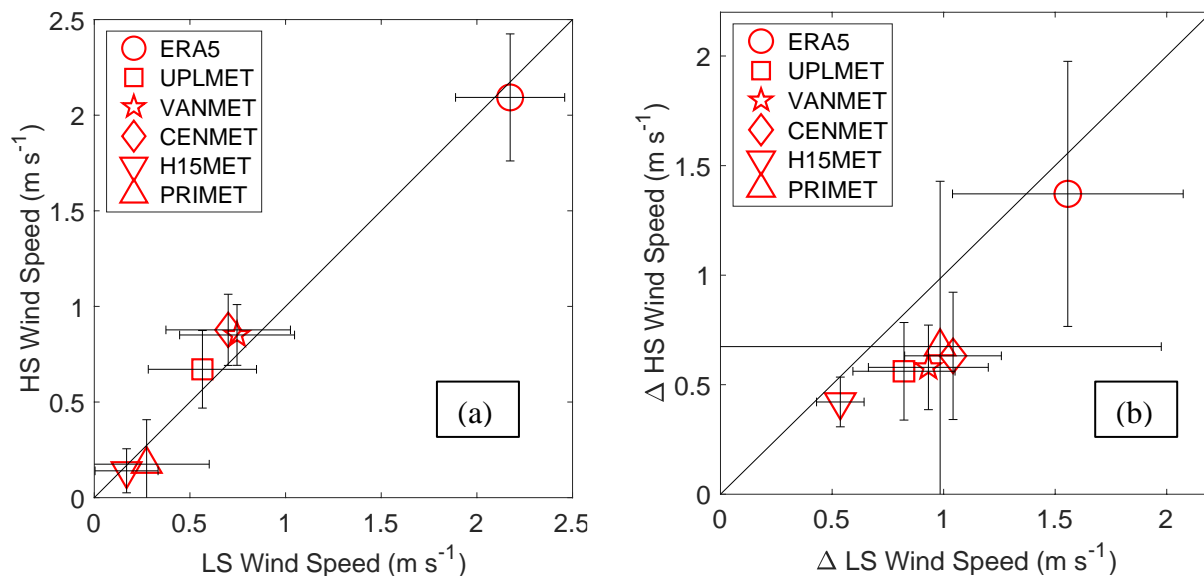
460 Wind speed during the study period increased with elevation and ERA5-Land modeled
461 wind speed was approximately two times greater than wind speed measured by the benchmark
462 stations at 10-m height (Figure 10). Daily-averaged wind speed for stations over the period of the
463 study were similar on HS versus LS days at elevations ranging from 436 to 1298 m and from

464 ERA5-Land (Figure 10a), given by close proximity of data markers to the 1-to-1 diagonal. The
 465 bars showing ± 1 standard deviation for benchmark stations in Figure 10a indicate that variability
 466 in measured wind speed was greater for LS days compared to HS days, consistent with
 467 subcanopy measurements in WS1 (Figures 7a, 9a). This difference in wind speed variability,
 468 however, was not captured by the ERA5-Land analyses. Midday wind direction for all stations
 469 (not shown) was upvalley indicating that differential insolation on topography drives basin-scale
 470 windflow above the forest canopy for both LS and HS days. On days classified as low-stability,
 471 on average, wind speed increased more from 6 AM to the maximum wind speed in the afternoon,
 472 both at benchmark stations in canopy gaps and in the ERA-5 reanalysis, compared to high-
 473 stability days (Figure 10b). This result indicates that above-canopy mountain breezes accelerated
 474 more during LS days. Stronger acceleration of above-canopy winds and increased TKE on LS
 475 days relative to HS days moderates solar heating of the canopy and limits development of a
 476 within-canopy inversion and down-valley sub-canopy winds (Figure 7).

477 ERA5-Land pressure gradient and 10-m wind speed provide more support for increased
 478 mountain breeze development during LS days. The 00Z (16:00 PST) ERA5-Land surface
 479 pressure gradient averaged 2.5% greater on LS days versus HS days for the basin average. Since
 480 ERA5-Land gridded products represent averaged quantities for a given grid box, the actual
 481 pressure gradient difference over smaller, localized scales likely exceeds this value. An increased
 482 horizontal pressure gradient on LS days over the HJ Andrews region favored accelerating above-
 483 canopy wind speed and turbulence that would ventilate the canopy, decreasing thermal
 484 stratification through the canopy relative to HS days.

485 Collectively, these results illustrate that low stability days corresponded to days when
 486 above-canopy upslope winds directly influenced sub-canopy winds. During days with high in-
 487 canopy stability, above canopy winds tended to remain decorrelated from sub-canopy winds
 488 throughout the day.

489



490 Figure 10. Relationship of average wind speed on high stability days vs. low stability days in the
 491 study period (July 19, 2012 to September 17, 2012). (a) Average daily wind speed for HS and LS

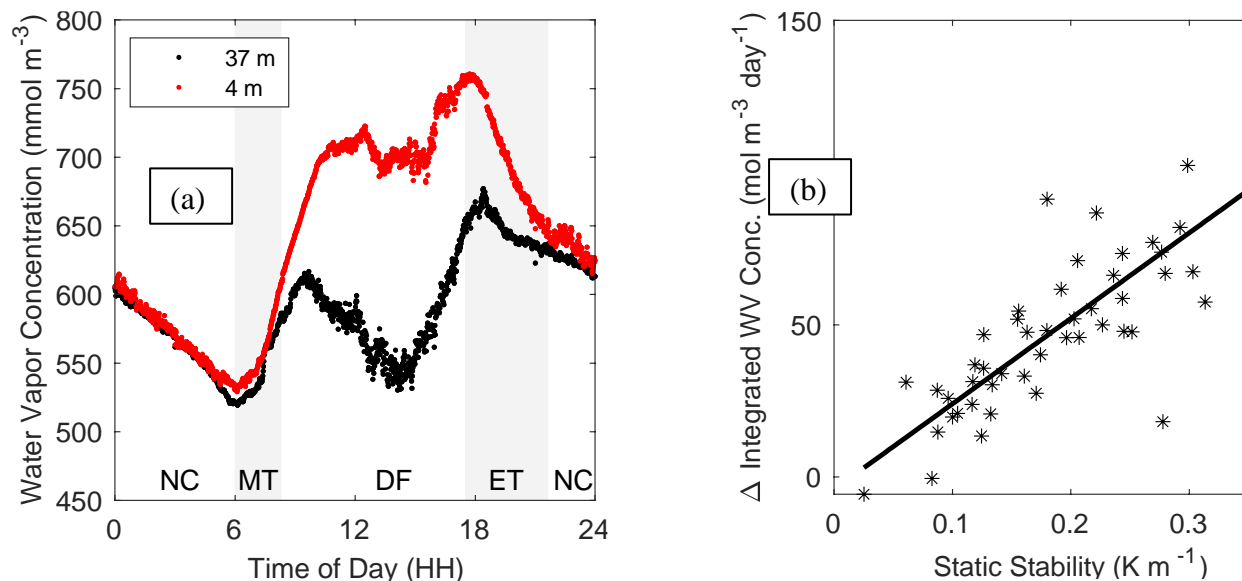
492 days, (b) average daily increase in wind speed from 6AM PST until the afternoon wind speed
 493 maximum from ERA5-Land (10-m winds) and at benchmark stations. Vertical and horizontal
 494 bars indicate one standard deviation, determined independently for each axis.

495 3.7 Moisture gradients and fluxes

496 The difference in daily-composited water vapor concentration between 4 m and 37 m
 497 reached its maximum during the DF period on high stability days (Figure 11 a). The gradient of
 498 virtual potential temperature, which already accounts for the water vapor influence on buoyancy,
 499 was 47% less than the potential temperature gradient between 4 m and 37 m agl at the WS1
 500 tower. So greater sub-canopy moisture decreased within-canopy static stability but not enough to
 501 erode the stable layer. Because total precipitation was low (31 mm) and infrequent (spread over 3
 502 days) during the study period (Figure 8), short term differences in vadose zone water available
 503 for evaporation or transpiration between HS and LS days were unlikely to account for the
 504 observed difference in water vapor concentrations above and below the canopy.

505 The difference in water vapor concentration between the generally moister sub-canopy
 506 and drier above-canopy air increased with sub-canopy static stability (Figure 11b; $R^2=0.67$). In
 507 other words, stronger within-canopy inversions are associated with greater sub-canopy humidity,
 508 relative to the air above the canopy. Lower latent heat flux on HS days relative to LS days both
 509 above and below the canopy (Fig 7c) as well as lower sub-canopy TKE imply that stronger
 510 within-canopy inversions on HS days constrain within-canopy mixing and vertical moisture flux
 511 out of the canopy. As vertical mixing is more constrained, subcanopy moisture concentration
 512 increases and, for a given downslope wind speed, more moisture is advected downslope by
 513 subcanopy winds.

514



515 Figure 11. Relationship of water vapor concentration to static stability. (a) Composited water
 516 vapor concentration over time during the day for high stability days at 4 m (red) and 37 m

517 (black). (b) Difference in average daily water vapor concentration, 4 m minus 37 m, versus the
518 daily maximum stability (1 hr averaged) for all days in the study period.

519 3.8 Wind speed and potential temperature along the watershed axis

520 The difference in sub-canopy wind speed was positively related to the difference in air
521 temperature between the two along-channel stations (B4 and C4) for HS days in the 50-day IOP
522 ($R^2=0.47$). The slope of the relationship suggests that a 1 m s^{-1} increase in wind speed
523 corresponds to a $3 \text{ }^\circ\text{C}$ increase in T_v between these two stations. An increase of 0.1 K m^{-1} in
524 static stability for the 12:30-13:30h period on high stability days is associated with a 0.3 m s^{-1}
525 increase in wind speed (Figure 7a), which in turn corresponds with a 1 K increase T_v between B4
526 and C4, well within the range measured during this experiment. Since sub-canopy wind speed
527 (Figure 7a) and water vapor concentration (Figure 11b) both increase with increasing stability, an
528 increase in static stability produces a positive feedback of water vapor advection through the
529 subcanopy space. For example, for a 0.1 K m^{-1} increase in dry static stability produces a 17%
530 diagnosed increase in water vapor transport by downslope winds relative to the observations (see
531 also the supplement, Section S5).

532 4 Discussion

533 The presented results document a flow regime within a PNW coniferous forest that
534 adjusts to the relative intensity of within-canopy static stability. Wind above the canopy can
535 more easily mix with subcanopy air on days when within-canopy stability is low, thereby
536 producing larger latent heat fluxes through the canopy than on days when within-canopy stability
537 is greater. In contrast, strong within-canopy stability restrains vertical moisture flux and
538 engenders increased subcanopy humidity and increased downslope moisture advection. To the
539 authors' knowledge, these linkages between within-canopy stability and vertical vs. downslope
540 vapor transport are a novel finding for forested regions. A linear cause and effect paradigm does
541 not fully describe the development of LS vs. HS days because, for example, greater through-
542 canopy mixing weakens stability, which further promotes vertical moisture flux, reinforcing an
543 LS condition. On HS days, increased downslope moisture advection in a plantation forest
544 changes the distribution of moisture relative to convective mixing. These findings may provide a
545 mechanism to explain observed higher summer evapotranspiration in conifer plantations reported
546 by Perry and Jones (2017), Grondahl et al. (2019) and Segura et al. (2020).

547 Comparing the results of this study with previous studies, the strongest subcanopy
548 downslope winds occurred under the highest stability conditions. However, Wang et al. (2015)
549 found the strongest down-valley winds during moderate stability regimes in a temperate,
550 deciduous forest valley (Wang et al., 2015). Differences in slope and forest canopy structure in
551 this study likely account for different findings compared to Wang et al. (2015). For example,
552 Moon et al. (2019) and Thomas (2011) found large variability in subcanopy wind speed profiles
553 and other statistics caused by variations in canopy structure. Valley configuration (width and
554 depth) also affects the strength of downslope flow and resulting development of a cold air pool
555 (Kiefer & Zhong, 2015). In unvegetated mountains, under high-pressure conditions typical of
556 summer in the Pacific Northwest of the US, local winds convey heat and water vapor upslope
557 during the day, but downslope at night (e.g. Oke, 2002; Geiger, 2009). However, results of this
558 study show that under high pressure conditions, the presence of a forest canopy creates a within-
559 canopy inversion, which strengthens the buoyancy force that drives flow down the slope and

560 enables downslope winds to persist for much of the daytime. TKE and latent heat flux profiles
561 for LS days (Fig 7b) are indicative of above-canopy coherent structures that disturb the sub-
562 canopy air space and promote the loss of sub-canopy moisture by the ejection-sweep process
563 (Finnigan, 1979; Shaw et al., 1983; Thomas et al., 2008).

564 When considering broader implications of the observations detailed in this study we
565 acknowledge that regional climate models (RCMs) do not resolve the subcanopy wind regime.
566 However, RCMs have skill to predict how climate forcings may change under different climate
567 scenarios and thereby influence sub-canopy moisture transport processes. Regional climate
568 model (~25-km resolution) runs under Representative Concentration Pathway (RCP) 4.5 project
569 an increasing summer/autumn 500 mb high pressure anomaly in the Pacific Northwest (PNW)
570 relative to areas outside of the western US (Rupp et al., 2017). Summer precipitation has been
571 declining since 1980 based on USHCN records for Oregon and Washington (Menne et al., 2009),
572 and is expected to continue to decrease (Rupp et al., 2017). These trends will increase air
573 temperature and vapor pressure and reduce relative humidity above the canopy during the
574 summer, decreasing surface latent heat flux while increasing sensible heat flux from PNW
575 forests. Increases in the ratio of sensible heat flux to latent heat flux (Bowen ratio) increase the
576 strength of mountain breezes (Alpert & Mandel, 1986; De Ridder & Gallée, 1998). Therefore,
577 the increased sensible heat flux over PNW forests predicted by Rupp et al. (2017) would be due
578 not only to energy repartitioning from latent to sensible heat (which is resolvable by an RCM)
579 but also due to increased within-canopy mixing as a consequence of increased surface layer wind
580 speed (which is not resolvable by an RCM). This finding implies that regional climate warming
581 over PNW forests will reduce sub-canopy moisture, potentially limiting moisture-mediated
582 microclimate refugia in these seasonally dry conifer forests (e.g., Davis et al., 2019).

583 Treating sensible heat flux as an independent variable, increased diabatic heating on a
584 PNW coniferous forest should increase the strength of the mountain breeze on LS days.
585 However, interdependencies of environmental variables and feedbacks between them are not
586 fully understood so we also consider the possibility that winds at canopy level weaken, allowing
587 a strengthened within-canopy inversion. The physical rationale for considering this alternative is
588 that regionally predicted lower relative humidity may increase partitioning of solar insolation
589 into sensible heat, leading to increased warming at canopy level and thereby strengthening the
590 within-canopy inversion on days when above canopy winds do not increase. One can diagnose
591 the increase in wind speed and water vapor concentration as static stability increases on HS days
592 from the slope of the regression that relates wind speed to dry static stability on HS days (Figure
593 7a) and the slope of the regression that relates water vapor concentration to dry static stability
594 (Figure 11b). Combining these equations allows one to estimate the increase in downslope water
595 vapor transport as static stability increases on HS days. In summary, RCM trends support
596 increasing latent heat flux through the forest canopy on days with low within-canopy stability
597 and increasing downslope advective flux on days with high within-canopy stability.

598 **5 Conclusions**

599 In this intensive field study in a 45-yr-old conifer plantation in a steep mountain valley in
600 Oregon, USA, heating of the forest canopy produced within-canopy inversions, whose strength
601 regulated a bi-modal sub-canopy wind regime during the dry season. On days with relatively
602 weak canopy heating and within-canopy temperature inversions, above canopy winds more
603 efficiently mix subcanopy air, leading to greater than average vertical moisture flux and weaker

604 than average along-slope, sub-canopy water vapor advection. On days with relatively strong
 605 canopy heating and within-canopy temperature inversion, vertical moisture flux is suppressed
 606 and daytime downslope winds are stronger than average under the canopy.

607 Increased downslope advection redistributes sub-canopy water vapor and other
 608 atmospheric constituents from upslope to downslope areas, providing an alternate method of
 609 drying the sub-canopy environment that is not resolved in regional models. Regional-scale
 610 increases in Bowen ratio predicted by a regional climate model suggest that both vertical and
 611 horizontal water vapor transport from the forest will be enhanced as the climate warms. These
 612 findings have implications for how plantation forests respond to climate change.

613 Future work shall include determining how forest stand structure and landscape patterns
 614 interact with wind regimes and climate fluctuations. Building on the methods in this study,
 615 further work is needed to resolve spatially distributed pressure gradients and air parcel
 616 trajectories into and out of forested mountain valleys to enhance understanding of sub-canopy
 617 wind regimes.

618 **Acknowledgments, Samples, and Data**

619 The authors declare that they have no conflict of interest with other affiliations. Funding:
 620 this study was supported by NSF Award #0955444 (PI: CKT); funding to the HJ Andrews Forest
 621 Long-Term Ecological Research (LTER) program (NSF 1440409, NSF 0823380) and U.S.
 622 Forest Service Pacific Northwest Research Station support of hydrology and climate records at
 623 the H.J. Andrews Experimental Forest. PI HJO acknowledges partial support by NSF Physical
 624 and Dynamic Meteorology (PDM) Grant No. 1848019. SAD acknowledges partial support in the
 625 form of startup funding from the University of Nevada, Reno. Benchmark station data (Daly &
 626 McKee, 2019) are available as data set MS001 through the Andrews Data Catalog
 627 (<http://andlter.forestry.oregonstate.edu/data/catalog/datacatalog.aspx>). IOP station data Thomas
 628 (2017) are available as data set MV007 through the Andrews Data Catalog.

629 **References**

- 630 Alpert, P., & Mandel, M. (1986). Wind variability—An indicator for a mesoclimatic change in
 631 Israel. *Journal of Applied Meteorology and Climatology*, 25(11), 1568-1576.
 632 [https://doi.org/10.1175/1520-0450\(1986\)025<1568:WVIFAM>2.0.CO;2](https://doi.org/10.1175/1520-0450(1986)025<1568:WVIFAM>2.0.CO;2)
- 633 Argerich, A., Haggerty, R., Johnson, S. L., Wondzell, S. M., Dosch, N., Corson-Rikert, H.,
 634 Ashkenas, L. R., Pennington, R., & Thomas, C. K. (2016). Comprehensive multiyear
 635 carbon budget of a temperate headwater stream. *Journal of Geophysical Research-*
 636 *Biogeosciences*, 121(5), 1306-1315. <https://doi.org/10.1002/2015JG003050>
- 637 Brutsaert, W., & Parlange, M. B. (1992). The unstable surface layer above forest: Regional
 638 evaporation and heat flux. *Water Resources Research*, 28(12), pp.3129-3134.
 639 <https://doi.org/10.1029/92WR01860>
- 640 Campbell Scientific, Inc. (2015). RM Young Wind Monitor Instruction Manual.
- 641 Daly, C., Conklin, D. R., & Unsworth, M. H. (2010). Local atmospheric decoupling in complex
 642 topography alters climate change impacts. *International Journal of Climatology*, 30(12),
 643 1857-1864. <https://doi.org/10.1002/joc.2007>

- 644 Daly, C., & McKee, W. (2019). Meteorological data from benchmark stations at the Andrews
645 Experimental Forest, 1957 to present. Corvallis, OR: Long-Term Ecological Research.
646 Forest Science Data Bank. doi:10.6073/pasta/c96875918bb9c86d330a457bf4295cd9
- 647 Davis, K. T., Dobrowski, S. Z., Holden, Z. A., Higuera, P. E., & Abatzoglou, J. T. (2019).
648 Microclimatic buffering in forests of the future: the role of local water
649 balance. *Ecography*, 42(1), 1-11. <https://doi.org/10.1111/ecog.03836>
- 650 Davis, R., Yang, Z., Yost, A., Belongie, C., & Cohen, W. (2017). The normal fire environment—
651 Modeling environmental suitability for large forest wildfires using past, present, and
652 future climate normals. *Forest Ecology and Management*, 390, 173-186.
653 <https://doi.org/10.1016/j.foreco.2017.01.027>
- 654 de Frenne, P., Lenoir, J., Luoto, M., Scheffers, B. R., Zellweger, F., Aalto, J., ... & Hylander, K.
655 (2021). Forest microclimates and climate change: Importance, drivers and future research
656 agenda. *Global Change Biology*, 27(11), 2279-2297.
- 657 De Ridder, K., & Gallée, H. (1998). Land surface-induced regional climate change in southern
658 Israel. *Journal of Applied Meteorology*, 37(11), 1470-1485. [https://doi.org/10.1175/1520-0450\(1998\)037<1470:LSIRCC>2.0.CO;2](https://doi.org/10.1175/1520-0450(1998)037<1470:LSIRCC>2.0.CO;2)
- 660 Dobrowski, S. Z. (2011). A climatic basis for microrefugia: the influence of terrain on
661 climate. *Global Change Biology*, 17(2), pp.1022-1035. <https://doi.org/10.1111/j.1365-2486.2010.02263.x>
- 663 Ferrez, J., Davison, A. C., & Rebetez, M. (2011). Extreme temperature analysis under forest
664 cover compared to an open field. *Agricultural and Forest Meteorology*, 151(7), 992-
665 1001. <https://doi.org/10.1016/j.agrformet.2011.03.005>
- 666 Finnigan, J. J. (1979). Turbulence in waving wheat. II. Structure of momentum
667 transfer. *Boundary-Layer Meteorology*, 16(3), 213-236. doi:10.1007/BF03335367
- 668 Fredriksen, R. L. (1970). Erosion and sedimentation following road construction and timber
669 harvest on unstable soils in three small western Oregon watersheds. Research Papers.
670 Pacific Northwestern Forest and Range Experiment Station, (PNW-104).
- 671 Freundorfer, A., Rehberg, I., Law, B. E., & Thomas, C. (2019). Forest wind regimes and their
672 implications on cross-canopy coupling. *Agricultural and Forest Meteorology*, 279,
673 107696. <https://doi.org/10.1016/j.agrformet.2019.107696>
- 674 Frey, S. J., Hadley, A. S., Johnson, S. L., Schulze, M., Jones, J. A., & Betts, M. G. (2016).
675 Spatial models reveal the microclimatic buffering capacity of old-growth forests. *Science*
676 *Advances*, 2(4), e1501392. doi:10.1126/sciadv.1501392
- 677 Froelich, N. J., & Schmid, H. P. (2006). Flow Divergence and Density Flows above and below a
678 Deciduous Forest: Part II. Below-Canopy Thermotopographic Flows. *Agricultural and*
679 *Forest Meteorology*, 138. <https://doi.org/10.1016/j.agrformet.2006.03.013>
- 680 Geiger, R., Aron, R.H. & Todhunter, P. (2009). The climate near the ground. Rowman &
681 Littlefield.
- 682 Gronsdahl, S., Moore, R. D., Rosenfeld, J., McCleary, R. & Winkler, R. (2019). Effects of
683 forestry on summertime low flows and physical fish habitat in snowmelt-dominant

- 684 headwater catchments of the Pacific Northwest. *Hydrological Processes*, 33(25),
685 pp.3152-3168. <https://doi.org/10.1002/hyp.13580>
- 686 Halpern, C. B., & Franklin, J. F. (1990). Physiognomie development of Pseudotsuga forests in
687 relation to initial structure and disturbance intensity. *Journal of Vegetation Science*, 1(4),
688 475-482. <https://doi.org/10.2307/3235781>
- 689 Hansen, M. C., Potapov, P. V., Moore, R., Hancher, M., Turubanova, S. A., Tyukavina, A.,
690 Thau, D., Stehman, S. V., Goetz, S. J., Loveland, T. R. & Kommareddy, A. (2013). High-
691 resolution global maps of 21st-century forest cover change. *Science*, 342(6160), pp.850-
692 853. doi:10.1126/science.1244693
- 693 Harr, R. D. (1983). Potential for augmenting water yield through forest practices in Western
694 Washington and Western Oregon 1. *Journal of the American Water Resources*
695 *Association*, 19(3), 383-393. <https://doi.org/10.1111/j.1752-1688.1983.tb04595.x>
- 696 Hersbach, H., Bell, B., Berrisford, P., Hirahara, S., Horányi, A., Muñoz-Sabater, J., et al. (2020).
697 The ERA5 global reanalysis. *Quarterly Journal of the Royal Meteorological Society*,
698 146(730), 1999–2049. <https://doi.org/10.1002/qj.3803>
- 699 Hicks, B. J., Beschta, R. L., & Harr, R. D. (1991). Long-term changes in streamflow following
700 logging in Western Oregon and associated fisheries implications 1. *Journal of the*
701 *American Water Resources Association*, 27(2), 217-226. <https://doi.org/10.1111/j.1752-1688.1991.tb03126.x>
- 703 Holden, Z. A., Swanson, A., Klene, A. E., Abatzoglou, J. T., Dobrowski, S. Z., Cushman, S. A.,
704 Squires, J., Moisen, G. G. and Oyler, J. W. (2016). Development of high-resolution (250
705 m) historical daily gridded air temperature data using reanalysis and distributed sensor
706 networks for the US Northern Rocky Mountains. *International Journal of*
707 *Climatology*, 36(10), pp.3620-3632. <https://doi.org/10.1002/joc.4580>
- 708 Hood, E., Gooseff, M. N., & Johnson, S. L. (2006). Changes in the character of stream water
709 dissolved organic carbon during flushing in three small watersheds, Oregon. *Journal of*
710 *Geophysical Research-Biogeosciences*, 111(G1). <https://doi.org/10.1029/2005JG000082>
- 711 Hosker, R. P., Jr., Nappo, C. P., Jr., & Hanna, S. R. (1974). Diurnal Variation of the Thermal
712 Structure in a Pine Plantation. *Agricultural Meteorology*, 13, 259–265.
713 [https://doi.org/10.1016/0002-1571\(74\)90053-3](https://doi.org/10.1016/0002-1571(74)90053-3)
- 714 Hughes, L. (2000). Biological consequences of global warming: is the signal already
715 apparent? *Trends in Ecology & Evolution*, 15(2), 56-61. [https://doi.org/10.1016/S0169-5347\(99\)01764-4](https://doi.org/10.1016/S0169-5347(99)01764-4)
- 717 Jones, J. A. & Hammond, J. C. (2020). River management response to multi-decade changes in
718 timing of reservoir inflows, Columbia River Basin, USA. *Hydrological*
719 *Processes*, 34(25), pp.4814-4830. <https://doi.org/10.1002/hyp.13910>
- 720 Juang, J. Y., Katul, G. G., Siqueira, M., Stoy, P. C., Palmroth, S., McCarthy, H. R., Kim, H. S.,
721 & Oren, R. (2006). Modeling nighttime ecosystem respiration from measured CO₂
722 concentration and air temperature profiles using inverse methods. *Journal of Geophysical*
723 *Research-Atmospheres*, 111(D8). <https://doi.org/10.1029/2005JD005976>

- 724 Karlsson, I. M. (2000). Nocturnal air temperature variations between forest and open
725 areas. *Journal of Applied Meteorology*, 39(6), 851-862. [https://doi.org/10.1175/1520-0450\(2000\)039<0851:NATVBF>2.0.CO;2](https://doi.org/10.1175/1520-0450(2000)039<0851:NATVBF>2.0.CO;2)
726
- 727 Kiefer, M. T. & Zhong, S. (2013). The effect of sidewall forest canopies on the formation of
728 cold-air pools: A numerical study. *Journal of Geophysical Research:
729 Atmospheres*, 118(12), pp.5965-5978. <https://doi.org/10.1002/jgrd.50509>
- 730 Kiefer, M. T. & Zhong, S. (2015). The role of forest cover and valley geometry in cold-air pool
731 evolution. *Journal of Geophysical Research: Atmospheres*, 120(17), pp.8693-8711.
732 <https://doi.org/10.1002/2014JD022998>
- 733 Launiainen, S., Vesala, T., Mölder, M., Mammarella, I., Smolander, S., Rannik, Ü., Kolari, P.,
734 Hari, P., Lindroth, A. & Katul, G. (2007). Vertical variability and effect of stability on
735 turbulence characteristics down to the floor of a pine forest. *Tellus B*, 59(5), pp.919-936.
736 <https://doi.org/10.1111/j.1600-0889.2007.00313.x>
- 737 Lefsky, M. A., Cohen, W. B., Acker, S. A., Parker, G. G., Spies, T. A., & Harding, D. (1999).
738 Lidar remote sensing of the canopy structure and biophysical properties of Douglas-fir
739 western hemlock forests. *Remote Sensing of Environment*, 70(3), 339-361.
740 [https://doi.org/10.1016/S0034-4257\(99\)00052-8](https://doi.org/10.1016/S0034-4257(99)00052-8)
- 741 Lembrechts, J. J. and Lenoir, J. (2020). Microclimatic conditions anywhere at any time! *Global
742 Change Biology*, 26(2), pp.337-339.
- 743 Lenoir, J., Hattab, T., & Pierre, G. (2017). Climatic microrefugia under anthropogenic climate
744 change: implications for species redistribution. *Ecography*, 40(2), 253-266.
745 <https://doi.org/10.1111/ecog.02788>
- 746 Leuzinger, S., & Körner, C. (2007). Tree species diversity affects canopy leaf temperatures in a
747 mature temperate forest. *Agricultural and Forest Meteorology*, 146(1-2), 29-37.
748 <https://doi.org/10.1016/j.agrformet.2007.05.007>
- 749 Lundquist, J. D., Pepin, N. and Rochford, C. (2008). Automated algorithm for mapping regions
750 of cold-air pooling in complex terrain. *Journal of Geophysical Research:
751 Atmospheres*, 113(D22). <https://doi.org/10.1029/2008JD009879>
- 752 Menne, M. J., Williams Jr., C. N., & Vose, R. S. (2009). The US Historical Climatology
753 Network monthly temperature data, version 2. *Bulletin of the American Meteorological
754 Society*, 90(7), 993-1008. <https://doi.org/10.1175/2008BAMS2613.1>
- 755 Minder, J. R., Mote, P. W. and Lundquist, J. D. (2010). Surface temperature lapse rates over
756 complex terrain: Lessons from the Cascade Mountains. *Journal of Geophysical
757 Research: Atmospheres*, 115(D14). <https://doi.org/10.1029/2009JD013493>
- 758 Moon, K., Duff, T. J., & Tolhurst, K. G. (2019). Sub-canopy forest winds: understanding wind
759 profiles for fire behaviour simulation. *Fire Safety Journal*, 105, 320-329.
760 <https://doi.org/10.1016/j.firesaf.2016.02.005>
- 761 Moore, G. W., Bond, B. J., Jones, J. A., Phillips, N., & Meinzer, F. C. (2004). Structural and
762 compositional controls on transpiration in 40- and 450-year-old riparian forests in western
763 Oregon, USA. *Tree Physiology*, 24(5), 481-491.
764 <https://doi.org/10.1093/treephys/24.5.481>

- 765 Muñoz-Sabater, J., Dutra, E., Agustí-Panareda, A., Albergel, C., Arduini, G., Balsamo, G.,
766 Boussetta, S., Choulga, M., Harrigan, S., Hersbach, H., Martens, B., Miralles, D. G.,
767 Piles, M., Rodríguez-Fernández, N. J., Zsoter, E., Buontempo, C., Thépaut, J-N.
768 (2021). ERA5-Land: A state-of-the-art global reanalysis dataset for land applications.
769 Earth System Science Data Discussions. Copernicus GmbH, 1–50.
770 <https://doi.org/10.5194/essd-2021-82>
- 771 Nadeau, D. F., Pardyjak, E. R., Higgins, C. W., et al. (2012). Flow during the evening transition
772 over steep Alpine slopes. *Quarterly Journal of the Royal Meteorological Society*,
773 139:607–624. <https://doi.org/10.1002/qj.1985>
- 774 Nadeau, D. F., Oldroyd, H. J., Pardyjak E. R., et al. (2018). Field observations of the morning
775 transition over a steep slope in a narrow alpine valley. *Environmental Fluid Mechanics*,
776 1-22. <https://doi.org/10.1007/s10652-018-9582-z>
- 777 NOAA National Centers for Environmental Information, State of the Climate: Drought for
778 Annual 2012, published online January 2013, retrieved on January 3, 2021,
779 <https://www.ncdc.noaa.gov/sotc/drought/201213>.
- 780 Oke, T. R. (2002). Boundary layer climates. Routledge. (p. 178-179).
- 781 Oldroyd, H. J., Pardyjak, E. R., Higgins, C. W., & Parlange, M. B. (2016). Buoyant Turbulent
782 Kinetic Energy Production in Steep-Slope Katabatic Flow. *Boundary-Layer Meteorology*,
783 161:405–416. <https://doi.org/10.1007/s10546-016-0184-3>
- 784 Perry, T. D., & Jones, J. A. (2017). Summer streamflow deficits from regenerating Douglas-fir
785 forest in the Pacific Northwest, USA. *Ecohydrology*, 10(2), e1790.
786 <https://doi.org/10.1002/eco.1790>
- 787 Pypker, T. G., Unsworth, M. H., Lamb, B., Allwine, E., Edburg, S., Sulzman, E., Mix, A. C. &
788 Bond, B. J. (2007). Cold air drainage in a forested valley: Investigating the feasibility of
789 monitoring ecosystem metabolism. *Agricultural and Forest Meteorology*, 145(3-4), 149-
790 166. <https://doi.org/10.1016/j.agrformet.2007.04.016>
- 791 Raynor, G. S. (1971). Wind and temperature structure in a coniferous forest and a contiguous
792 field. *Forest Science*, 17(3), 351-363. <https://doi.org/10.1093/forestscience/17.3.351>
- 793 Ritchie, M. W., Skinner, C. N., & Hamilton, T. A. (2007). Probability of tree survival after
794 wildfire in an interior pine forest of northern California: effects of thinning and
795 prescribed fire. *Forest Ecology and Management*, 247(1-3), 200-208.
796 <https://doi.org/10.1016/j.foreco.2007.04.044>
- 797 Rupp, D. E., Li, S., Mote, P. W., Shell, K. M., Massey, N., Sparrow, S. N., ... & Allen, M. R.
798 (2017). Seasonal spatial patterns of projected anthropogenic warming in complex terrain:
799 a modeling study of the western US. *Climate Dynamics*, 48(7-8), 2191-2213.
800 [doi:10.1007/s00382-016-3200-x](https://doi.org/10.1007/s00382-016-3200-x)
- 801 Rupp, D. E., Shafer, S. L., Daly, C., Jones, J. A., & Frey, S. J. (2020). Temperature gradients and
802 inversions in a forested Cascade Range basin: Synoptic-to local-scale Controls. *Journal*
803 *of Geophysical Research: Atmospheres*, 125(23), e2020JD032686.
804 <https://doi.org/10.1029/2020JD032686>

- 805 Schmidli, J. (2013). Daytime heat transfer processes over mountainous terrain. *Journal of the*
806 *Atmospheric Sciences*, 70:4041–4066. <https://doi.org/10.1175/JAS-D-13-083.1>
- 807 Segura, C., Bladon, K. D., Hatten, J. A., Jones, J. A., Hale, V. C. and Ice, G. G. (2020). Long-
808 term effects of forest harvesting on summer low flow deficits in the Coast Range of
809 Oregon. *Journal of Hydrology*, 585, p.124749.
810 <https://doi.org/10.1016/j.jhydrol.2020.124749>
- 811 Shaw, R. H., Tavangar, J., & Ward, D. P. (1983). Structure of the Reynolds stress in a canopy
812 layer. *Journal of Climate and Applied Meteorology*, 22(11), 1922-1931.
813 [https://doi.org/10.1175/1520-0450\(1983\)022<1922:SOTRSI>2.0.CO;2](https://doi.org/10.1175/1520-0450(1983)022<1922:SOTRSI>2.0.CO;2)
- 814 Staebler, R. M., & Fitzjarrald, D. R. (2005). Measuring canopy structure and the kinematics of
815 subcanopy flows in two forests. *Journal of Applied Meteorology*, 44(8), 1161-1179.
816 <https://doi.org/10.1175/JAM2265.1>
- 817 Stull, R. B. *An Introduction to Boundary Layer Meteorology* (Vol. 13). Springer Science &
818 Business Media, 2012.
- 819 Thomas, C., & Foken, T. (2007). Flux contribution of coherent structures and its implications for
820 the exchange of energy and matter in a tall spruce canopy. *Boundary-Layer Meteorology*,
821 123(2), 317-337. <https://doi.org/10.1007/s10546-006-9144-7>
- 822 Thomas, C., Martin, J. G., Goeckede, M., Siqueira, M. B., Foken, T., Law, B. E., ... & Katul, G.
823 (2008). Estimating daytime sub-canopy respiration from conditional sampling methods
824 applied to multi-scalar high frequency turbulence time series. *Agricultural and Forest*
825 *Meteorology*, 148(8-9), 1210-1229. <https://doi.org/10.1016/j.agrformet.2008.03.002>
- 826 Thomas, C. K. (2011). Variability of sub-canopy flow, temperature, and horizontal advection in
827 moderately complex terrain. *Boundary-Layer Meteorology*, 139(1), 61-81.
828 <https://doi.org/10.1007/s10546-010-9578-9>
- 829 Thomas, C. K., & Smoot, A. R. (2013). An effective, economic, aspirated radiation shield for air
830 temperature observations and its spatial gradients. *Journal of Atmospheric and Oceanic*
831 *Technology*, 30(3), 526-537. <https://doi.org/10.1175/JTECH-D-12-00044.1>
- 832 Thomas, C. K., Martin, J. G., Law, B. E., & Davis, K. (2013). Toward biologically meaningful
833 net carbon exchange estimates for tall, dense canopies: multi-level eddy covariance
834 observations and canopy coupling regimes in a mature Douglas-fir forest in
835 Oregon. *Agricultural and Forest Meteorology*, 173, 14-27.
836 <https://doi.org/10.1016/j.agrformet.2013.01.001>
- 837 Thomas, C. (2017), Advanced Resolution Canopy FLOW (ARCFLO) experiment employing the
838 SUBcanopy Sonic Anemometer Network (SUSAN) in WS01 of the HJ Andrews
839 Experimental Forest, July-September 2012. Long-Term Ecological Research. Forest
840 Science Data Bank, Corvallis, OR.
841 [doi:10.6073/pasta/e1dcac713961e62c3aaad2816bbf7780](https://doi.org/10.6073/pasta/e1dcac713961e62c3aaad2816bbf7780)
- 842 Tóta, J., Roy Fitzjarrald, D., & da Silva Dias, M. A. (2012). Amazon rainforest exchange of
843 carbon and sub-canopy air flow: Manaus LBA site—A complex terrain condition. *The*
844 *Scientific World Journal* 2012. <https://doi.org/10.1100/2012/165067>

- 845 Vickers, D., & Thomas, C. K. (2013). Some aspects of the turbulence kinetic energy and fluxes
846 above and beneath a tall open pine forest canopy. *Agricultural and Forest Meteorology*,
847 181, 143–151. <https://doi.org/10.1016/j.agrformet.2013.07.014>
- 848 Vickers, D., & Thomas, C. K. (2014). Observations of the scale-dependent turbulence and
849 evaluation of the flux–gradient relationship for sensible heat for a closed Douglas-fir
850 canopy in very weak wind conditions. *Atmospheric Chemistry and Physics*, 14(18),
851 9665–9676. <https://doi.org/10.5194/acp-14-9665-2014>
- 852 Wang, X., Wang, C., & Li, Q. (2015). Wind regimes above and below a temperate deciduous
853 forest canopy in complex terrain: Interactions between slope and valley
854 winds. *Atmosphere*, 6(1), 60-87. <https://doi.org/10.3390/atmos6010060>
- 855 Whiteman, C. D. (1982). Breakup of temperature inversions in deep mountain valleys: Part I.
856 Observations. *Journal of Applied Meteorology*, 21(3), 270-289.
857 [https://doi.org/10.1175/1520-0450\(1982\)021<0270:BOTIID>2.0.CO;2](https://doi.org/10.1175/1520-0450(1982)021<0270:BOTIID>2.0.CO;2)
- 858 Whiteman, C. D. (1990). Observations of thermally developed wind systems in mountainous
859 terrain. In *Atmospheric processes over complex terrain* (pp. 5-42). *American*
860 *Meteorological Society*, Boston, MA. https://doi.org/10.1007/978-1-935704-25-6_2